13

Influence of surface oxidation and interfaces on the magnetic properties of the $Co/Al_2O_3/Co$ system

© A.V. Kobyakov,[1,2] G.S. Patrin,[1,2] V.I. Yushkov,[1,2] D.A. Ivanov,[1,2] V.A. Komarov,[1,2] R.Yu. Ridenko[1]

[1]Siberian Federal University,
660041 Krasnoyarsk, Russia
[2]Kirensky Institute of Physics, Krasnoyarsk Scientific Center, Siberian Branch, Russian Academy of Sciences,
660036 Krasnoyarsk, Russia
e-mail: nanonauka@mail.ru

Received July 11, 2025
Revised August 7, 2025
Accepted August 8, 2025

The magnetic behavior of three-layer $Co/Al_2O_3/Co$ samples obtained by the magnetron sputtering method with variable thickness of the oxide layer from 3 to 8 nm and constant thicknesses of the magnetic cobalt layers of 10 nm has been studied. Contributions to the magnetic behavior from the upper oxidized surface of cobalt (Co–CoO interface), interlayer interaction of cobalt layers and effects due to defects at the Co/Al_2O_3 and Al_2O_3/Co interfaces have been analyzed. A negative exchange bias was detected at low temperatures. The temperature at which a step-like hysteresis loop appeared increased with increasing oxide layer thickness

Keywords: interface, ferromagnet, oxide layer, interlayer interaction, exchange bias.

DOI: 10.61011/TP.2026.02.62894.178-25

Introduction

Ferromagnetic(FM)/non-magnetic (NM)/ferromagnetic three-layer structures are critical spintronic devices. Conductors, semiconductors, metal oxides and other layers are used as a non-magnetic layer. Such structures have good prospects for application and are already used as magnetic reading sensors in hard disks and magnetic memory cells, for magnetoresistive random access memory (MRAM), for flexible electronic devices and other applications [1–4]. The system is also interesting for fundamental research in the solid state physics, in particular, for investigating phenomena associated with charge, spin and heat transfer through an oxide layer [5–7].

FM/NM/FM structures can have unique properties. For example, a change in their resistance can result from antiparallel magnetization equalization in FM-layers or vortex configuration of free layer configuration [8]. In the case when a change in resistance is made sufficiently large, and the field necessary for magnetization equalization is made sufficiently small, then the structure comes to be a very sensitive magnetic field detector. Antiferromagnetic (AFM) coupling between FM-layers is also an object of keen experimental and theoretical interest. In many structures, oscillatory coupling of FM-layers occurs depending on the NM thickness. In most theoretical models, oscillation periods are determined by the Fermi surface properties of NM material. Oscillation periods measured on samples grown by the molecular-beam epitaxy method are in good agreement with predictions of these theories in the following systems: Cr/Fe [9], Mo/Fe [10], Cu/Co [11], Cu/Fe [12], Pd/Fe [13], Au/Fe [14], Al/Fe [14].

Generally, FM/NM/FM structures can have bilinear exchange interaction when there is collinear arrangement of magnetizations in FM-layers, biquadratic exchange interaction when there is noncollinear arrangement of magnetizations in FM-layers and/or twisted domain structures [15]. On the other hand, it is not quite understood how interface alloying affects the interlayer interaction. Interaction mechanism is unclear due to difficulties in the description of very complex interfaces between layers. In addition, the interface itself along with the intermediate layer contribution will affect the electric conductivity behavior. In addition, in thin multilayer systems with an AFM/FM or FM/AFM interface, there can be an exchange bias effect or hysteresis loop shift along the magnetic field axis.

In [16], A.R. Fert et al. demonstrated a spin-polarized tunnel junction with a NiO–Co–AlO_x-Co film structure. The team was focused on magnetic layer anisotropy, exchange bias effect and coupling between two magnetic electrodes depending on various NiO film preparation conditions. The study obtained a stable result, more than 20 % TMR (tunnel magnetoresistance) at room temperature along the easy axis. It was later shown [17] that the spin polarization in Co-AlO_x–Co magnetic tunnel junctions was controlled by the interphase atomic structure and emerging chemical coupling, and the interphase oxygen adsorption may be the key factor leading to positive spin polarization in the Co–AlO_x–Co system. Thus, ferromagnetic layer oxidation control in aluminum oxide tunnel junctions is of paramount importance for achievement of a significant level of tunnel current spin-polarization.

Besides the magnetization loop shifts [5] and more complex magnetization loop shapes [18] for some systems,

asymmetric behavior is observed on the ascending and descending branches of hysteresis loop [19–21]. Hysteresis loop asymmetry may be associated with different types of magnetic rotation mechanisms for descending and ascending branches. Generally, one branch then relates to coherent rotation and the other branch relates to domain nucleation and domain wall movement [21–23]. In such studies, the origin of asymmetric hysteresis loops is associated with various causes, for example, higher order anisotropy [24]; irreversibility resulting from a training effect [25]; non-collinearity of FM and AFM-anisotropy axes [20]; inhomogeneity of laterally structured samples [26]; internal properties with collinear anisotropy [27]. It was also found that asymmetry can depend on the measurement angle, i.e. rotation can be more symmetric when the field is applied along the hard axis [22].

Note that the effect of various magnetic exchanges and anisotropy on generation and shape of skyrmions have been reviewed earlier in a FM/NM/FM multilayer structure in the form of disc [28]. In particular, it has been found that the RKKY coupling (Rudermann–Kittel–Kasuya–Iosida interaction) can determine whether skyrmions can be generated. However, the coupling doesn't have any significant effect on the skyrmion size. When the RKKY coupling appears to be weak, irregular cross-shaped domain states can be formed.

Thus, multilayer structures with the FM/NM interface have become promising candidates in the field of spintronics for extensive studies where the FM-layer interface can be considerably modified. As a result, very interesting magnetic behaviors can be observed for such multilayer systems. We study magnetic properties, in particular, exchange bias and magnetic interaction of FM-layers in a FM/NM/FM system with a variable oxide interlayer thickness. Cobalt (Co) was chosen as a ferromagnetic layer. Aluminum oxide (Al_2O_3) was chosen as a non-magnetic interlayer. We assumed that there were disordered spins at the interface. Therefore, it was decided to make stepped three-layer samples to explore each step. To explain magnetic behavior, a phenomenological FM-core–AFM-shell model is considered [29].

1. Materials and experimental procedure

This study investigated $Co/Al_2O_3/Co$ structures with an Al_2O_3 layer and magnetic Co layers. Films were applied to a glass substrate using the „Omicron NanoTechnology" ultrahigh vacuum magnetron sputtering system (Germany) with the „Pfeiffer Vacuum" turbomolecular pumps. The substrate is placed in a working chamber lift through a sample charging lock system. Substrate position in the lift with respect to the magnetron was set to ~ 20 cm. Deposition was performed at a basic pressure of 10^{-10} Torr in 3 mTorr argon (with in-process film growth thickness control). The substrate was preliminary cleaned by ion-plasma etching in the working chamber directly before the

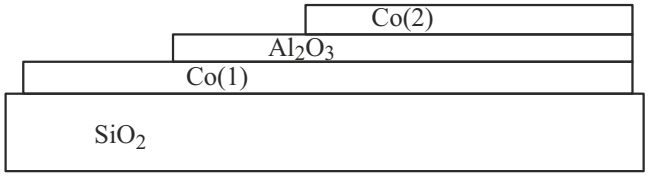

Figure 1. Configuration of $Co/Al_2O_3/Co$.

argon sputtering process. All layers were deposited on the rotating substrate at a substrate temperature of $T \approx 373$ K.

The aluminum oxide layer was deposited by an AC-powered magnetron using an Al_2O_3 (99.99 %) target. The Co layer was deposited by a DC-powered magnetron using a Co (99.95 %) target. All targets are made by „SCOTECH LIMITED" UK.

A series of samples with a variable Al_2O_3 thickness from 3 nm to 8 nm was produced for the study. An Al_2O_3/Co sample with Al_2O_3thickness of 5 nm was additionally made in the same conditions. Thicknesses of all Co layers were constant — 10 nm. Deposition rates were: Al_2O_3 — 0.55 nm/min, Co — 7.2 nm/min. The Al_2O_3 barrier layer was grown on a Co layer with a thickness from 3 nm at a low rate, which is indicative of a sharp interface between Al_2O_3 and the lower layer. Deposition rate was controlled by the power supplied to the magnetron. Film thickness was measured *in situ* using a calibrated thickness measuring quartz crystal. To explore magnetic properties in more detail, samples were made using a dedicated sliding shutter designed to form stepped films. The shutter worked *in situ*. Configuration of the samples is shown in Figure 1. Points, in which measurements were made, will be named as follows: the first Co layer surface — „Co(1)", Al_2O_3 surface— „Al_2O_3", point on the upper Co layer — „Co(2)".

Surface morphology of all samples, including the clean glass surface, was examined using the VeecoMultiMode atomic force microscope (resolution 1 nm). Phase composition was investigated by the X-ray diffraction method (XRD) using the DRON-4-07 unit. X-ray diffraction reflection intensity was examined using the ICDD PDF 4+ crystallographic database.

Magnetic measurements were performed using the magneto-optic Kerr effect (NanoMOKE-2) and SQUID-magnetometer (MPMS-XL). Regardless of the fact that Co was deposited on the rotating substrate, a small magnetic anisotropy occurred in samples with an exposed Co surface. To determine the easy axis orientation more accurately, the magneto-optic Kerr effect method was used: the sample rotated from 0 to 3600 at room temperature and magnetization loops were read every 50 loop. Then the easy axis orientation was determined from the loop analysis. Then for all measurements, the magnetic field was directed in the sample plane along the easy axis.

The maximum magnetic field for the magneto-optic method and SQUID magnetometry was 1.5 kOe and 15 kOe, respectively. The temperature range in both

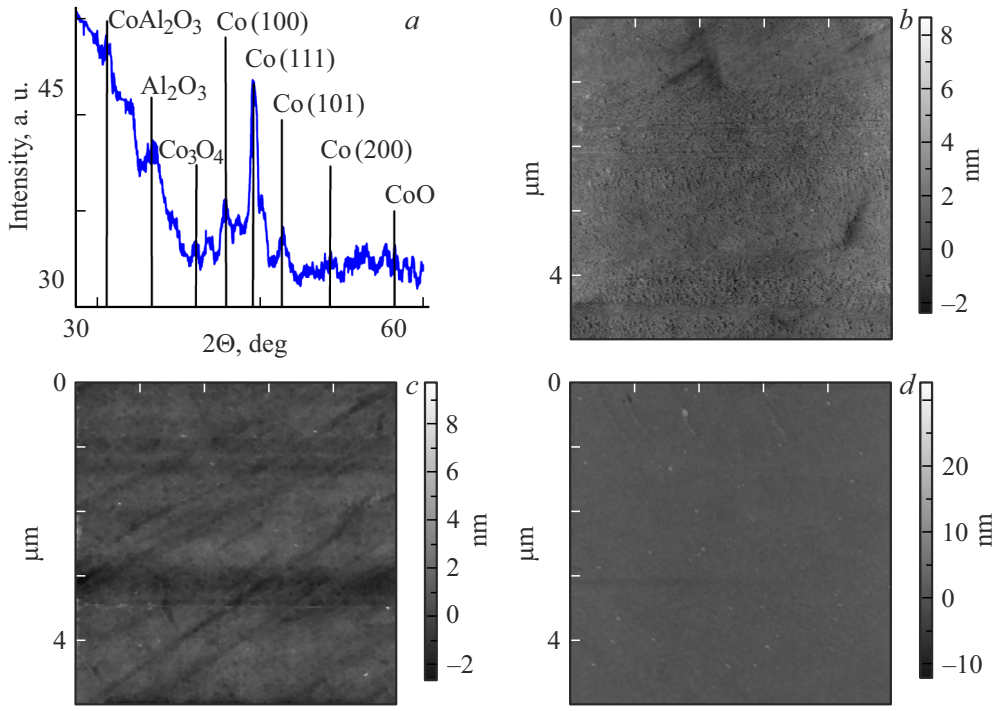

Figure 2. XRD image for the Co(10 nm)/Al_2O_3(8 nm)/Co(10 nm) sample (*a*), SEM images for the Co/Al_2O_3(3 nm)/Co samples: Co(1) surface (*b*), Al_2O_3 surface (*c*), Co(2) surface (*d*).

Mean roughness*Ra* and mean pellet diameter *d* on surfaces (Figure 1)

Sample	Surface	*Ra*, nm	*d*, nm
Co/Al_2O_3(3 nm)/Co	Co(1)	0.27	18
	Al_2O_3	0.29	30
	Co(2)	0.3	28
Co/Al_2O_3(5 nm)/Co	Co(1)	0.35	22
	Al_2O_3	0.4	18
	Co(2)	0.3	27
Co/Al_2O_3(8 nm)/Co	Co(1)	0.3	18
	Al_2O_3	0.45	16
	Co(2)	0.3	27

cases was from 4.2 to 300 K. The magneto-optic Kerr effect method was used to measure the magnetization loop characteristics by the procedure described in [30]. For measurements using the SQUID magnetometer, a film was first put into a demagnetizer before each measurement and then cooled in zero magnetic field (ZFC mode). As a result, hysteresis loops were measured for all samples. SQUID magnetometer was only used for measurements in three-layer parts of the samples. Magneto-optical measurements were conducted at each sample step.

2. Results and discussion

Figure 2, *a* shows X-ray images with a Al_2O_3 thickness equal to 8 nm. Diffraction peaks indicate that there are HCP ((100) and (101)) and FCC ((111) and (200)) phases of Co. There is a peak for Al_2O_3. The X-ray image shows the presence of noise, which may be assigned to the presence of small amounts of Co + O compounds (CoO and Co_3O_4) and Co + aluminum oxide compounds ($CoAl_2O_3$).

The table shows the AFM measurements of mean roughness *Ra* and pellet diameter *d* on the sample surfaces.

SEM images for Co/Al_2O_3(3 nm)/Co samples are shown in the figures: Co(1) surface (Figure 2, *b*), Al_2O_3 surface (Figure 2, *c*), Co(2) surface (Figure 2, *d*). Surface roughness of the upper Co layer in the Co/Al_2O_3/Co samples was approx. 0.3–0.4 nm. This suggest that the formed layers had a smooth top surface. In addition, note that surface roughness of the Al_2O_3 layer grows from 0.29 to 0.45 nm as the layer thickness grows. The size of pellets on the Al_2O_3 layer decreases from 30 to 16 nm. The same surface roughness evolution in the Al_2O_3 layer was observed earlier as Al_2O_3 was grown on Si substrates from the initial growth stage to a layer thickness of 23 nm with an increase in roughness from 0.25 to 0.4 nm [31]. And the evolution of Al_2O_3 pellet sizes is probably associated with the appearance of new nucleation centers during the Al_2O_3 film growth, thus leading to formation of many finer grains. Moreover, thinner Al_2O_3 films have more interconnected pores, while thicker films are usually more dense and have less pores [32]. This

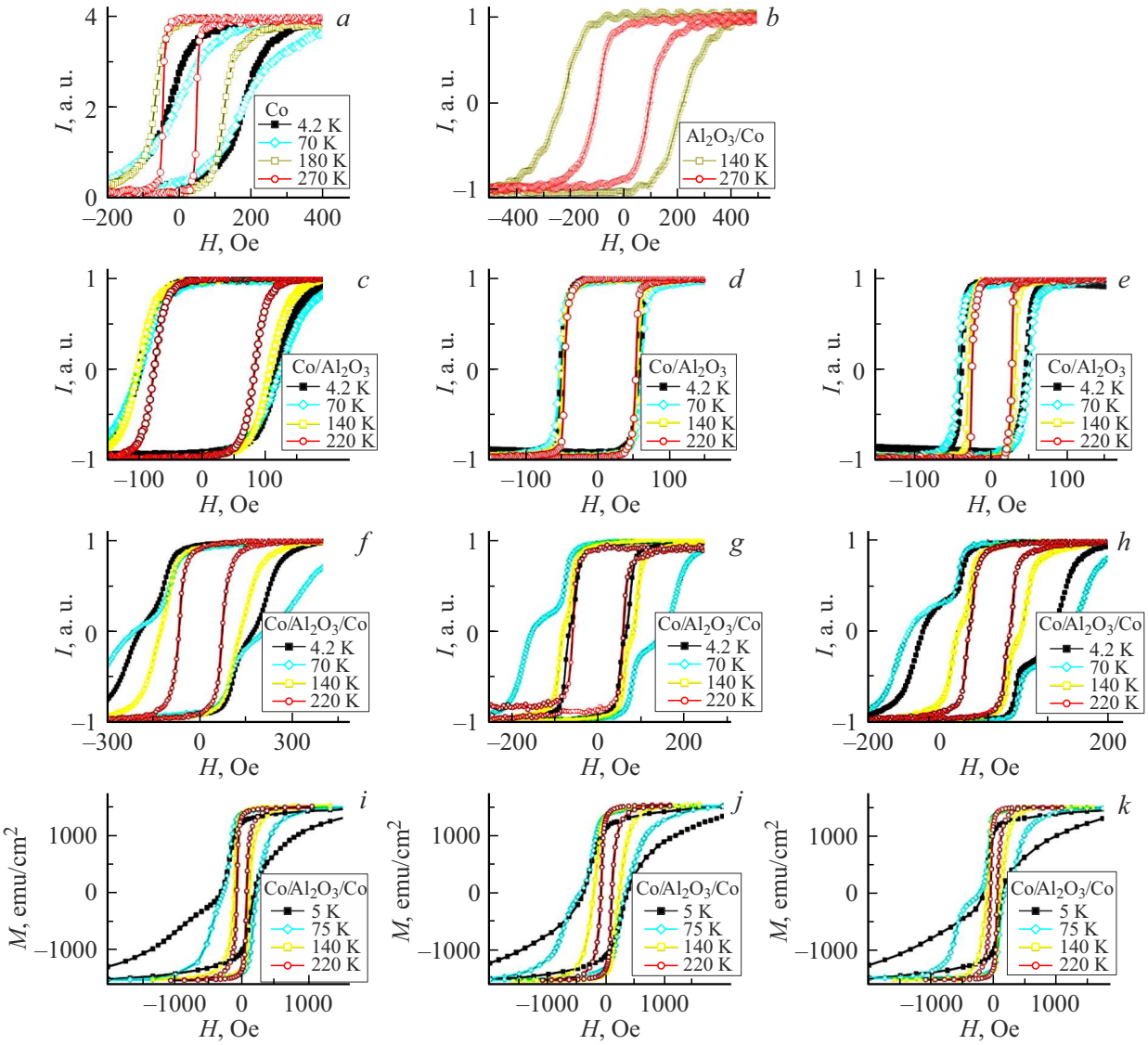

Figure 3. Local magnetization loops measured using the Kerr effect for the $Co/Al_2O_3/Co$ system on surfaces (Figure 1): *a* — (Co(1)), *b* — (Al_2O_3/Co), *c*–*e* — (Al_2O_3), *f*–*h* — (Co(2)). Integral magnetization loops measured using the SQUID magnetometry of the $Co/Al_2O_3/Co$ three-layer film: (*i*–*k*). Al_2O_3 layer thicknesses: 3 nm (*c*,*f*,*i*), 5 nm (*d*,*g*,*j*) and 8 nm (*e*,*h*,*k*). *I* — MOKE signal intensity, *M* — magnetization.

affects considerable reduction of pellet sizes. Thus, at different Al_2O_3 thicknesses, the Al_2O_3/Co interface will have different effect on behavior of $Co/Al_2O_3/Co$ in a magnetic field.

Figure 3 shows hysteresis loops measured on each step surface. Results for the Co(1) surface are shown in Figure 3, *a*. Results for the separate Al_2O_3/Co film are shown in Figure 3, *b*. Results for the Al_2O_3 surface are shown in Figure 3, *c*–*e*. Results for the Co(2) surface obtained using the magneto-optic Kerr effect method are shown in Figure 3, *f*–*h*, and SQUID magnetometer measurements are shown in Figure 3, *i*, *j*, *k*. Figures show the measurements at 4.2–300 K for samples with the following Al_2O_3 interlayer thicknesses: 3 nm (Figure 3, *c*,*f*,*i*), 5 nm (Figure 3, *d*,*g*,*j*), 8 nm (Figure 3, *e*,*h*,*k*).

For a single Co film (Co(1) surface, Figure 3, *a*), two effects occur: exchange bias of the hysteresis loop and change in the loop shape below 180 K, which are apparently associated with the appearance of cobalt oxides on the surface because such bias is not observed on the Co film covered by Al_2O_3 (Figure 3, *c*–*e*). These effects were explored earlier in [29]. It was shown that a photoelectron spectrum measured on a Co surface consisted of main components typical of Co (a fraction equal to 49.7 % — $2p_{3/2}$) and oxygen components (a fraction equal to 41.6 %), namely, CoO and Co_3O_4 (antiferromagnetic materials with Neel temperatures in the bulk state of $T_N \sim 290$ K and 40 K, respectively). Here, appearance of the exchange bias during cooling confirms that antiferromagnetic CoO particles have been

formed. These particles occur when Co surface is oxidized.

Note that loops shift to the positive side during cooling in external zero magnetic field. This is not typical of the Co/CoO system. The loop shift direction is associated with many factors, in particular, with changes in electronic properties and material's structural configuration at the interface between Co and cobalt oxides such as CoO, Co_3O_4, defects and FM-core–AFM-shell pellets. This is caused by a complex interface coupling between Co particles and oxides, and depends on interface spins and oxide behavior. Positive exchange bias in Co with oxidized surface can occur only in certain conditions. For example, it was observed during field-cooling, when using the sample „training" effect and by other methods [5].

In [33], the SQUID magnetometry methods detected positive exchange bias in Co/CoO films during cooling in ZFC mode at 200−400 K followed by loop shift reduction. Cobalt was an amorphous material. The authors assigned the unusual positive shift at room temperature and below to the fact that sizes of various Co–CoO crystals in the film were not the same, therefore the crystal blocking temperature is distributed. Thus, there is competition between the magnetic moments of Co and CoO grains, which retain the AFM-structure. AFM-moments can be either in a low energy state or in a high energy state depending on the external magnetic field direction. Considering that the film crystals are not the same, these factors facilitate the emergence of positive bias.

Such situation was adequately interpreted by A.N. Dobrynin et al. [34]. The model of A.N. Dobrynin et al. implies that T_N is lower at the FM/AFM interface than in the rest of the AFM-layer. This causes mobility of interface AFM-spins near T_N, actually changing the sign of interface exchange coupling from plus to minus and, thus, inducing a positive exchange bias effect. The authors show that the positive exchange bias effect is determined by the exchange interaction within the AFM layer and competes with the FM–AFM exchange. Thus, such model may be used in cases when exchange interactions are quite weak for AFM grains to be remagnetized independently of their neighbors, but are sufficiently strong to affect magnetization processes, i.e. are equivalent to a magnetic field on the order of the measured bias field.

In [35], positive shift of the loop was found in the temperature range of 300 mK−80 K. For this, the external field was changed during measurement using the following procedure $0 \to (+H)$, $0 \to (-H)$, $0 \to (+H)$ .... In the paper, Co was a polycrystalline soft magnetic material with negligibly low volume-averaged magnetocrystalline anisotropy. The authors also assign the positive bias to a competition between the exchange and magnetostatic energies. Authors show that magnetization inhomogeneities can occur on the edges of a particle because of its shape, edge roughness and defects. Such inhomogeneities behave as remagnetization nucleation centers and can lead to a higher order effective anisotropy. Remagnetization is initiated by the nucleation process followed by domain wall propagation.

In our case, the presence (Figure 2, *a*) of HCP phases of Co (with the (100) and (101) planes in the lattice), FCC phases of Co (with the (111) planes (200) in the lattice), inhomogeneities in the form of CoO and Co_3O_4 produced as a result of natural oxidation, and the change in the external field during $0 \to (+H)$, $0 \to (-H)$, $0 \to (+H)$ ... measurement lead to a weak positive exchange bias. We have also observed the effect earlier [29] in Co with thicknesses of 10−40 nm when the bias decreased with Co thickness growth. However, at a Co thickness less than 10 nm, there was the negative exchange bias.

For a Co film coated with aluminum oxide (Al_2O_3 surface, Figure 3, *c*−*e* — Al_2O_3 thicknesses: 3, 5, 8 nm), the exchange bias effect is imperceptible. When the Al_2O_3 thickness is small, broadening of the hysteresis loop can be seen in Figure 3, *c*. There is a weak temperature dependence. Temperature dependence disappears at a thickness of 5 nm, and small broadening of the loop occurs at a thickness of 8 nm as the temperature decreases. This suggests that aluminum oxide protects the Co layer against oxidation, as a result field dependences are more rectangular.

It is known that in the XPS-spectrum, besides Al–O bonds, the presence of a core 2*p*-line of Al was also confirmed in an as-deposited film. This suggests that many broken bonds are formed in as-deposited Al_2O_3 films during deposition [36].

Al_2O_3 grows in the Volmer–Weber mode [37]. This implies that the Al_2O_3 films initially grow in the form of islands. Thus, Al–O islands contain much more aluminum than flat regions. Low temperature of the underlaying Co layer contributes to a short diffusion distance of these deposited atomic islands on the Co surface, which hinders their connection to form the layer. Multiple defects occur in a hyperfine layer after deposition. A hysteresis loop read from the Al_2O_3 surface appears to be a little broadened. As the temperature decreases during measurement, defects are activated (Figure 3, *c*). Then larger islands grow and become coupled to each other. Diameter of pellets on the surface decreases (see the Table). These connected islands are coated with hyperfine particles. This means that the growth pattern of the sputtered Al_2O_3 film changes from island to layer-by-layer growth mode. Mean roughness in this case increases (see the Table). However, it is more difficult to identify certain structure formation mechanisms because, when the magneto-optic Kerr effect method records hysteresis loops from local film areas.

Then note that measurements by the Kerr effect method use a 6350 Å helium-neon laser, which generally penetrates the Co film to a depth of 20−30 nm [38]. Therefore, for three-layer samples (Co/Al_2O_3/Co), a hysteresis loop can contain a combined loop of both lower and upper Co layers (Figure 3, *f*−*h*). Loops measured using the SQUID magnetometry also have a combined hysteresis loop (Figure 3, *i*, *j*, *k*).

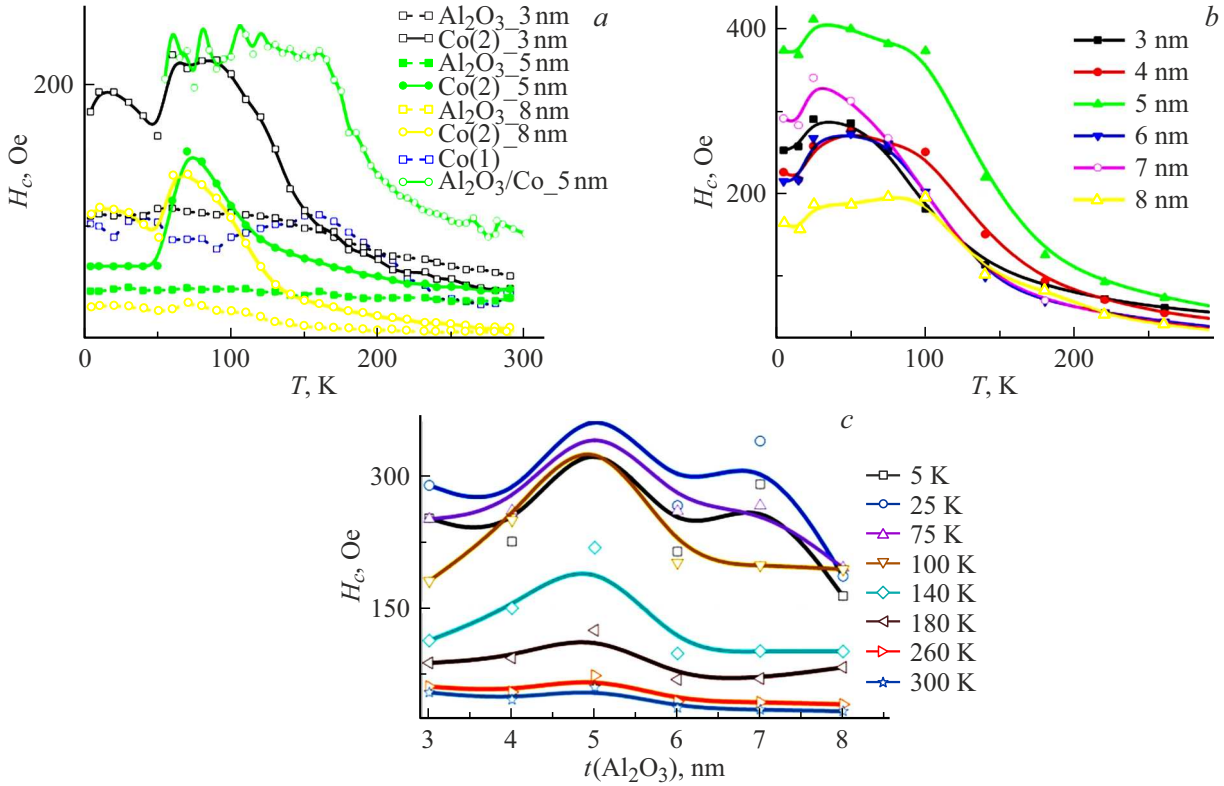

Figure 4. Temperature dependences of the coercive force for the $Co/Al_2O_3/Co$ system obtained from surfaces (Figure 1) Co(1), Al_2O_3, Co(2) and Al_2O_3/Co using the Kerr effect (a), for the $Co/Al_2O_3/Co$ three-layer film obtained using the SQUID magnetometer (b), and dependence of the Al_2O_3 interlayer thickness (c). Layer thicknesses Al_2O_3: 3, 5 and 8 nm.

As should be expected, hysteresis loops at room temperature were rectangular. As the temperature decreases, rectangularity disappears and a „stepped" configuration appears. At 25–50 K, the latter is most distinct. For samples with a 3 nm interlayer, the hysteresis loop got to be „stepped" as the temperature decreased below 50 K. As the interlayer thickness increases to 8 nm, this temperature grows to 140–220 K depending on the measurement method (Kerr effect or SQUID method).

When the Kerr effect method is used for measurement, hysteresis loops in fields up to 1.5 kOe are symmetric (Figure 3,f–h). When the SQUID magnetometry is used for measurement, symmetry of loops in fields up to 15 kOe disappears at temperatures below 50 K (Figure 3,i,j,k). Thus, an asymmetric loop has been found earlier [39] in the Co/Co_3O_4 film plane and perpendicularly to it in fields higher than 1 kOe at low temperatures. This was explained by oxygen ion implantation into thin Co films, which led to high magnetization outside the upper surface, and by training effects. Therefore, inhomogeneous oxidation of surface and interfaces and appearance of antiferromagnetic CoO or Co_3O_4 particles creating energy barriers for domain walls may contribute to the asymmetric loop in our case.

Temperature measurements of hysteresis loops provided the dependences of the coercive force $H_c = (|H1| + |H_2|)/2$ and exchange bias field $H_E = (H_1 - H_2)/2$ on temperature for all Al_2O_3 interlayer thicknesses. H_1 and H_2 correspond to magnetic fields, at which magnetizations change their sign as the magnetic field strength decreases and increases, respectively.

Figure 4,a shows temperature dependences of coercive force at each step of the sample measured using the Kerr effect for various Al_2O_3 interlayer thicknesses (3, 5, 8 nm) and the separate Al_2O_3/Co sample. Figure 4,b shows dependences of coercive forces on temperature for all Al_2O_3 layer thicknesses measured using the SQUID magnetometry.

Results demonstrate that increase in coercive forces takes place in all cases below 250 K. However, for the three-layer sample ($Co/Al_2O_3/Co$), H_c increases much more abruptly and becomes ~ 2 times as high as for a single Co layer at 4.2–100 K (a line in Figure 4,a for Co(1)). This fact indicates an additional contribution to magnetic interaction through the Al_2O_3 interlayer. In addition, Co deposited on Al_2O_3 has a coercive force (~ 80 Oe), which considerably exceeds that of the Co layer covered by Al_2O_3 (~ 30 Oe).

Figure 4,c shows the diagram of coercive forces vs. interlayer thickness. The diagram shows an increase in coercive force oscillations as the temperature decreases.

Figure 5,a shows temperature dependences of the exchange bias field at each step of the sample measured using the Kerr effect for various Al_2O_3 interlayer thicknesses (3, 5, 8 nm) and the separate Al_2O_3/Co sample. Figure 5,b

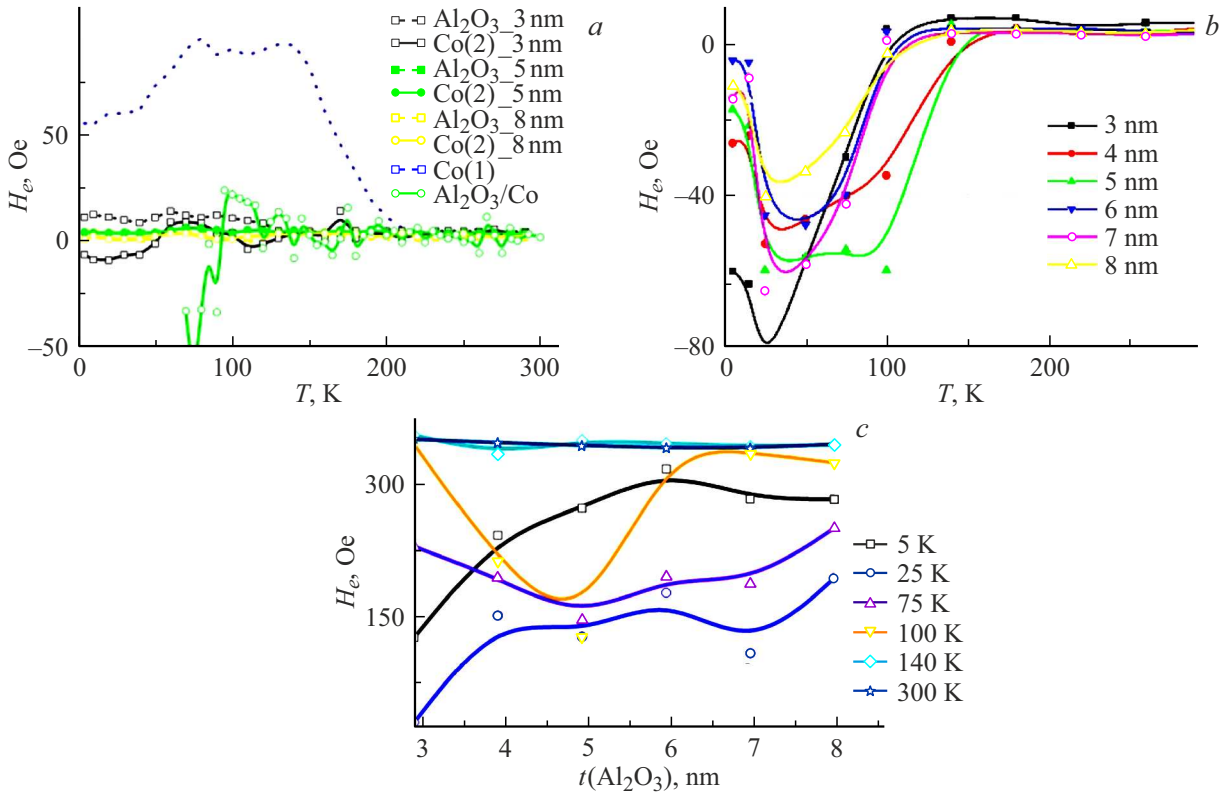

Figure 5. Temperature dependences of the exchange bias field for the Co/Al_2O_3/Co system obtained from surfaces (Figure 1) Co(1), Al_2O_3, Co(2) and Al_2O_3/Co using the Kerr effect (*a*), for the Co/Al_2O_3/Co three-layer film obtained using the SQUID magnetometer (*b*), and dependence of the Al_2O_3 interlayer thickness (*c*). Al_2O_3 layer thicknesses: 3, 5, and 8 nm.

shows temperature dependences of the exchange bias field for all Al_2O_3 layer thicknesses measured using the SQUID magnetometry.

Results obtained using the Kerr effect and SQUID magnetometry are different, which is to be expected. They are discussed in detail below.

When the Kerr effect is used for measurement, positive exchange bias 70−90 Oe is observed on a single Co layer, on surface Co(1). Exchange bias in the Co film covered with Al_2O_3 was not found. Exchange bias measured for the separate Al_2O_3/Co film is negative. Small negative exchange bias up to −10 Oe is observed for the Co/Al_2O_3(3 nm)/Co sample with its minimum near 25−50 K (for surface Co(2)). For other Al_2O_3 layer thicknesses, exchange bias is low-observable.

When the SQUID magnetometry is used for measurement, negative exchange bias with its minimum near 25−50 K occurs at temperatures below 100−150 K. As the Al_2O_3 interlayer thickness grows, exchange bias increases from −80 to −40 Oe in the temperature range of 25−50 K. Consequently, a diagram of exchange bias vs. interlayer thickness was drawn (Figure 5, *c*). The diagram shows an increase in exchange bias oscillations at temperatures below 140 K.

For the Co/Al_2O_3(5 nm)/Co sample, broadening of the exchange bias minimum should be noted (Figure 5, *b*) in the range of 50−100 K. It is known that effective lifetime of minority carriers is maximum for the Al_2O_3 film with a thickness of 5 nm [40]. The authors relate this to passivation of the Al_2O_3 layer due to a decrease in the interface recombination rate and in the density of dangling bonds at the substrate/Al_2O_3 interface. The same mechanism is possible in our case. This will lead to a change in exchange interaction between magnetic layers near the Al_2O_3 thickness of 5 nm.

Comparison of results obtained by the SQUID magnetometry and Kerr effect methods indicates a competitive mode of mechanisms behind the exchange bias effect and an activation mechanism responsible for magnetic state generation. Moreover, the results show that there are both FM-exchange between magnetic layers through a non-magnetic intermediate layer at temperatures close to room temperature and AFM-exchange at low temperatures. As the interlayer thickness increases, the exchange bias tends to zero for the whole temperature range. Figure 5, *c* shows that the exchange bias oscillates with the interlayer thickness at ∼ 1−2 nm intervals depending on temperature.

In the case when the Kerr effect is used, the main contribution to the hysteresis loop shall be given by the nearest layer, i.e. the upper Co layer. This layer has surface oxidation (antiferromagnetic particles, hence the exchange bias shall occur on the loop measured by this method.

However, a small shift of the three-layer film is observed only at the minimum interlayer thickness.

The Kerr effect method measures magnetic data from the surface magnetic layer because the beam of light cannot penetrate deeply into a sample (usually max. 20−30 nm). For the exchange bias to appear the antiferromagnetic thickness shall be at least 2−3 nm. In addition, if oxidation is nonuniform or partial, the Kerr effect averages the signal over the laser spot area. However, this is not observed on the single Co layer where the exchange bias achieves 80 Oe below 150 K. Therefore, it is hard to describe the disappearance of the exchange bias in the three-layer film (Figure 5, *a* — Co(2)), where the total Co thickness is about 20 nm, only by nonuniform small oxidation or by „local effects“Ėspecially that the negative shift is still observed as the interlayer thickness increases in the case of SQUID magnetometry measurements. Note that any large exchange bias from the Co/Al_2O_3 interface was not recorded, and a negative loop shift was observed for the Co/Al_2O_3 film.

It is known that the Kerr effect and SQUID magnetometry methods have different sensitivity to bulk and surface effects. Thus, the SQUID magnetometry measures the „total magnetic moment“ of the whole sample, including the contribution from all layers and interfaces, and even weak effects, if they contribute to the total magnetic moment. For example, in our case indirect exchange interaction between Co layers may occur through defects (roughness) in the barrier or spin tunneling through Al_2O_3. Alternately, if one of the Co layers have partially oxidized boundaries, this can lead to the exchange bias resulting from interaction between the ferromagnetic (Co) and antiferromagnetic (CoO) materials.

In [41], a model of uncompensated spins was proposed as an extension of Meiklejohn's and Bean's model with quantitative consideration of exchange bias fields on the basis of experimentally determined number of fixed moments and their sizes. In [42], it was shown that in the case of particular pellet sizes the exchange bias of the $Co/CoO–Al_2O_3$ system approaches 0 Oe unlike Co/CoO–MgO and Co/CoO [42]. Moreover, SQUID, which acts in higher magnetic fields, is used to observe transitions between various magnetic states, which might not be exhibited in lower fields used in MOKE. And magneto-optic method (MOKE), being a surface method, can „average“ the effects induced by inhomogeneities and local changes in magnetic structure leading to a more symmetric loop. Therefore, in the case of the Kerr effect measurement we presumably get some „compensated“ hysteresis loop.

In this case the upper Co–CoO interface, interaction between the Co layers and effects induced by defects at the Al_2O_3/Co interface contribute to magnetic behavior of the three-layer film. Interaction (ferromagnetic or antiferromagnetic) force and sign depend on the barrier thickness. Increase in the barrier thickness (Al_2O_3) from 3 to 8 nm will define the extent to which the Co layers are magnetically interconnected.

Thus, strong interlayer interaction occurs in the case of thin Al_2O_3 barrier (about 3−4 nm). However, spin tunneling or exchange interaction between Co layers (with a non-ideal rough barrier) is possible. The upper Co–CoO layer fixes the lower Co layer through Al_2O_3. SQUID magnetometry will show the exchange bias (up to 10−100 Oe) because both Co layers are coupled and CoO facilitates the effect. At low temperatures, the hysteresis loop is asymmetric. The Kerr effect will be used to record a compensated hysteresis loop.

In the case of mean Al_2O_3 barrier thickness (5−6 nm), the exchange interaction between Co layers decreases. CoO contribution still exists, but decreases as the Al_2O_3 thickness grows. Surface roughness of Al_2O_3 increases, defects appear at the interface, i.e. pellets are formed — ferromagnetic Co core with naturally oxidized CoO shell [29]. Pellets make additional contribution to the exchange bias. However, oscillations induced by RKKY-like interaction are observed (Figure 4, *c* and *5*, *c*). The Kerr effect will be used to record a partially „compensated“ hysteresis loop. In the case when the upper Co–CoO layer is nonuniform, the shift can disappear due to signal averaging.

In the case of a thick barrier (7−8 nm), layer „uncoupling“ occurs. The Co layers are now almost magnetically isolated. In the Kerr effect, the contribution from the upper Co–CoO layer and Al_2O_3/Co interface now grows. A small shift (1−10 Oe) occurs at higher temperatures (220 K, Figure 3, *h*). In the case of the SQUID magnetometry, the lower Co layer gives a symmetric loop and a small negative exchange bias from the Al_2O_3/Co interface still exists.

Note that behavior of magnetic properties in the Co/Al_2O_3(3 nm)/Co sample is similar to synthetic antiferromagnetism (SAF) [43]. Low coercive force (H_c = 10−50 Oe (Figure 4, *b*)). A linear segment in weak fields (magnetization almost doesn't grow to the critical field (Figure 3, *i*)). In Figure 3, *i*, at 5 K a part of the loop is almost linear with a abrupt transition to saturation. In Figure 3, *f*, there are abrupt shifts (spikes) at 4.2−100 K — a sign of concerted domain behavior. In this case strong antiferromagnetic interaction through the tunnel exchange equalizes the spins in adjacent Co layers in opposite directions.

Figure 6 shows dependences of the saturation field (Figure 6, *a*) and saturation magnetization M_s (Figure 6, *b*).

Figure 6, *a* shows that the saturation field depends on the Al_2O_3 layer thickness. H_S oscillates as the Al_2O_3 thickness increases, which is more pronounced as the temperature decreases below 100 K. Figure 6, *b* shows that the saturation magnetization also oscillates as the Al_2O_3 layer thickness grows throughout the temperature range.

It is hard to estimate the exchange interaction in the case of indirect exchange coupling of 3*d*-layers. It is not possible to identify all contributions from the experimental data. In addition, various types of exchange interaction between magnetic moments may exist: „orange-peel“ coupling (Neel coupling), indirect exchange coupling (exchange coupling

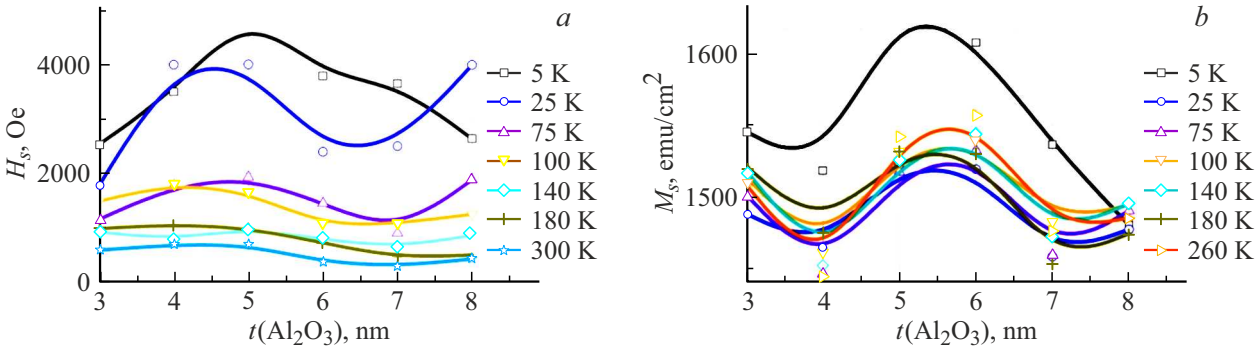

Figure 6. Dependence of the saturation field (*a*) and saturation magnetization (*b*) on the Al_2O_3 interlayer thickness.

by conduction electrons), anticorrelated dipole-dipole coupling and magnetostatic coupling [44,45].

Conclusion

The study uses the SQUID magnetometry and magneto-optic Kerr effect methods to examine magnetic behavior of Co/Al_2O_3/Co. three-layer samples. Contribution to magnetic behavior occur from several factors. Firstly, the positive exchange bias is induced by the upper oxidized Co surface (Co–CoO interface). Secondly, interaction of Co layers causes additional anisotropy. Thirdly, the Al_2O_3/Co and Co/Al_2O_3 interfaces and defects on them give rise to at least two effects. Appearance of the negative exchange bias from the Al_2O_3/Co interface, on which pellets are formed —a ferromagnetic Co core with a naturally oxidized CoO shell. Temperature independence of the lower Co layer depending on the Al_2O_3 thickness. Exchange interaction oscillations between magnetic layers as the Co/Al_2O_3 interface grows. Interaction (ferromagnetic or antiferromagnetic) force and sign depend on the barrier thickness and vary at low temperatures.

At Al_2O_3 thicknesses of 3−4 nm, there are: strong exchange interaction due to the Co layer coupling, contribution from the CoO interface and weak contribution from the Al_2O_3/Co interface.

At Al_2O_3 thicknesses of 5−6 nm, there are: a decrease in the interlayer interaction and increase in contribution from the Al_2O_3/Co interface due to interface thickness growth.

At Al_2O_3 thicknesses of 7−8 nm: indirect exchange interaction is minimized, contributions from the Al_2O_3/Co interface, CoO surface and „uncoupled“ Co layers prevail.

The findings may be of interest for production of multilayer structures designed for data storage, sensors and other devices.

Funding

The study was carried out under the state assignment of the Siberian Federal University (No. FSRZ-2023-0008).

Conflict of interest

The authors declare no conflict of interest.

References

[1] D. Mazumdar, W. Shen, X. Liu, B.D. Schrag, M. Carter, G. Xiao. J. Appl. Phys., **103**, 113911 (2008). DOI: 10.1063/1.2939265
[2] R. Perricone, I. Ahmed, Z. Liang, M.G. Mankalale, X.S. Hu, C.H. Kim, M. Niemier, S.S. Sapatnekar, J.P. Wang. Conf. Exhibition (DATE), 972 (2017). DOI: 10.5555/3130379.3130612
[3] N. Locatelli, V. Cros, J. Grollier. Nat. Mater., **13**, 11 (2014). DOI: 10.1038/nmat3823
[4] J. Huang, W. Chen. Science, **25**, 105041 (2022). DOI: 10.1016/j.isci.2022.105041
[5] J. Nogués, J. Sort, V. Langlais, V. Skumryev, S. Surinach, J.S. Munoz, M.D. Baró. Phys. Rep., **422**, 65 (2005). DOI: 10.1016/j.physrep.2005.08.004
[6] U. Martens, T. Huebner, H. Ulrichs, O. Reimer, T. Kuschel et al. Commun Phys., **1**, 65 (2018). https://doi.org/10.1038/s42005-018-0063-y
[7] A.V. Kukharev, A.L. Danilyuk, V.E. Borisenko. Tech. Phys., **55** (9), 1311 (2010). DOI: 10.1134/S1063784210090136
[8] I.Yu. Pashenkin, E.V. Skorokhodov, M.V. Sapozhnikov, A.A. Fraerman, G.A. Kichin, K.A. Zvezdin. Tech. Phys., **68** (11), 1501 (2023). DOI: 10.61011/TP.2023.11.57501.171-23
[9] J. Unguris, R.J. Celotta, D.T. Pierce. Phys. Rev. Lett., **67**, 140 (1991). DOI: 10.1103/PhysRevLett.67.140
[10] Z.Q. Qiu, J. Pearson, A. Berger, S.D. Bader. Phys. Rev. Lett., **68**, 1398 (1992). DOI: 10.1103/PhysRevLett.68.1398
[11] M.T. Johnson S.T. Purcell, N.W.E. McGee, R. Coehoorn, J. van de Stegge, W. Hoving. Phys. Rev. Lett., **68**, 2688 (1992). DOI: 10.1103/PhysRevLett.68.2688
[12] W.R. Bennett, W. Schwarzacher, W. Egelhoff. J. Appl. Phys., **70**, 5881 (1991). DOI: 10.1063/1.350093
[13] Z. Celinski, B. Heinrich. J. Mag. Mag. Mater., **99**, L25 (1991). DOI: 10.1016/0304-8853(91)90043-A
[14] A. Fuss, S. Demokritov, P. Grunberg, W. Zinn. J. Mag. Mag. Mater., **103**, L221 (1992). DOI: 10.1016/0304-8853(92)90192-Q

[15] G.S.Patrin, Ya.A.Vakhitova, Ya.G.Shiyan, A.V.Kobyakov, V.I.Yushkov. Pis'ma v ZhTF, **51** (4), 46 (2025) (in Russian). https://doi.org/10.61011/PJTF.2025.04.59844.20134
[16] B. Diouf, L. Gabillet, A.R. Fert, D. Hrabovsky, V. Prochazka, E. Snoeck, J.F. Bobo J. Mag. Mag. Mater., **265**, 204 (2003). DOI: 10.1016/S0304-8853(03)00267-1
[17] K.D. Belashchenko, E.Y. Tsymbal, I. Oleynik, M. van Schilfgaarde. Phys. Rev. B, **71**, 224422 (2005). DOI: 10.1103/PhysRevB.71.224422
[18] A.M. Kharlamova, A.V. Makarov, A.V. Svalov, E.E. Shalygina. Phys. Solid State, **63**, 1662 (2021). DOI: 10.1134/S1063783421100140
[19] A.V. Svalov, O.A. Adanakova, A.N. Gorkovenko, V.N. Lepalovskij, E.A. Stepanova, N.V. Selezneva, V.O. Vas'kovskiy. J. Magn. Magn. Mater., **507**, 166839 (2020). DOI: 10.1016/j.jmmm.2020.166839
[20] Y. Liu, S.-G. Wang, Y. Li, N. Li, Sh. Liu, N. Chen, M.-Hua Li, G.-Hua Yu. Phys. Rev. B, **84**, 104436 (2011). DOI: 10.1103/PhysRevB.84.104436
[21] M. Gierlings, M.J. Prandolini, H. Fritzsche, M. Gruyters, D. Riegel. Phys. Rev. B, **65**, 092407 (2002). DOI: 10.1103/PhysRevB.65.092407
[22] O.V. Koplak, V.S. Gornakov, Y.P. Kabanov, E.I. Kunitsyna, I.V. Shashkov. JETP Lett., **109**, 722 (2019). DOI: 10.1134/S0021364019110092
[23] N. Chowdhury, W. Kleemann, O. Petracic S. Bedanta. Phys. Rev. B, **98**, 134440 (2018). DOI: 10.1103/PhysRevB.98.134440
[24] J. McCord, R. Schäfer, R. Mattheis, K.-U. Barholz. J. Appl. Phys., **93**, 5491 (2003). DOI: 10.1063/1.1562732
[25] S. Brems, D. Buntinx, K. Temst, C. Van Haesendonck, F. Radu, H. Zabel. Phys. Rev. Lett., **95**, 157202 (2005). DOI: 10.1103/PhysRevLett.95.157202
[26] K. Theis-Bröhl, T. Schmitte, V. Leiner, H. Zabel, K. Rott, H. Brückl, J. McCord. Phys. Rev. B, **67**, 184415 (2003). DOI: 10.1103/PhysRevB.67.184415
[27] T.A. Taaev, K.S. Khizriev, A.K. Murtazaev. Phys. Solid State, **62** (6), 954 (2020). DOI: 10.1134/S106378342006030X
[28] M. Xu, J. Zhang, D. Meng, R. Li. J. Phys. D: Appl. Phys., **54**, 305301 (2021). DOI: 10.1088/1361-6463/abfad7
[29] A.V. Kobyakov, G.S. Patrin, V.I. Yushkov, N.N. Kosyrev, V.A. Komarov, Y.V. Tomashevich, R.Yu. Rudenko. J. Vac. Sci. Technol. A, **42**, 053413 (2024). DOI: 10.1116/6.0003772
[30] N.N. Kosyrev, V.Yu. Yakovchuk, G.S. Patrin, V.A. Komarov, E.N. Volchenko, I.A. Tarasov. Tech. Phys. Lett., **47**, 107 (2021). DOI: 10.1134/S1063785021020097
[31] E.O. Filatova, L. Peverini, E. Ziegler, I.V. Kozhevnikov, P. Jonnard, J.-M. André. J. Phys.: Condens. Matter., **22**, 345003 (2010). DOI: 10.1088/0953-8984/22/34/345003
[32] Zh. Chai, J. Li, X. Lu, D. He. RSC Adv., **4**, 39365 (2014). DOI: 10.1039/C4RA04565C
[33] F. Tian, J. Guo, Q. Zhao, K. Li, K. Cao, Zh. Dai, K. Chang, X. Ke, M. Fang, Y. Zhang, Ch. Zhou, S. Yang. Mater. Lett., **293**, 129631 (2021). DOI: 10.1016/j.matlet.2021.129631
[34] A.N. Dobrynin, P. Warin, A. Vorobiev, D. Givord, J. Magn. Magn. Mater., 166707 (2020). DOI: 10.1016/j.jmmm.2020.166707
[35] M.J. Martínez-Pérez, B. Müller, D. Schwebius, D. Korinski, R. Kleiner, J. Sesé, D. Koelle. Supercond. Sci. Technol., **30**, 024003 (2017). DOI: 10.1088/0953-2048/30/2/024003
[36] J. García-Serrano, A.G. Galindo, U. Pal. Sol. Energy Mater. Sol. Cells, **82**, 291 (2004). DOI: 10.1016/j.solmat.2004.01.026
[37] X. Tang, Z. Li, H. Liao, J. Zhang. Coatings, **9** (5), 341 (2019). DOI: 10.3390/coatings9050341
[38] K. Sarathlal, D. Kumar, V. Ganesan, A. Gupta. Appl. Surf. Sci., **258**, 4116 (2012). DOI: 10.1063/1.4739271
[39] M. Wortmann, T. Samanta, M. Gaerner, M. Westphal, J. Fiedler, I. Ennen, A. Hütten, T. Blachowicz, L. Caron, A. Ehrmann. APL Mater., **11**, 121118 (2023). DOI: 10.1063/5.0183566
[40] M. Salem, I. Massoudi, A.M. Almessiere, A.L. Al-Otaibi, N.M. Alghamdi, M. Gaidi, M.A. El Khakani, K. Khirouni. J. Mater. Sci.: Mater. Electron, **28**, 15768 (2017). DOI: 10.1007/s10854-017-7470-9
[41] Ch. Ge, X. Wan, E. Pellegrin, Z. Hu, S.M. Valvidares, A. Barla, W.-I. Liang, Y.-H. Chu, W. Zou, Y. Du, Nanoscale, **5**, 10236 (2013). DOI: 10.1039/c3nr02013d
[42] H. Ohldag, A. Scholl, F. Nolting, E. Arenholz, S. Maat, A.T. Young, M. Carey, J. Stöhr. Phys. Rev. Lett., **91**, 017203 (2003). DOI: 10.1103/PhysRevLett.91.017203
[43] R.A. Duine, K.-J. Lee, Stuart S.P. Parkin, M.D. Stiles. Nature Physics, **14**, 217 (2018). DOI: 10.1038/s41567-018-0050-y
[44] T. Warnatz. *Magnetic properties of epitaxial metal/oxide heterostructures, Ph.D. thesis* (Uppsala University, 2021)
[45] J.J. de Vries. *Interlayer exchange coupling in magnetic multilayers: a systematic experimental study* (Applied Physics and Science Education, Technische Universiteit Eindhoven, 1996), DOI: 10.6100/IR470784

Translated by E.Ilyinskaya